Robotica (2022), **40**, pp. 1168–1187
doi:10.1017/S0263574721001004

CAMBRIDGE
UNIVERSITY PRESS

RESEARCH ARTICLE

FEA-based tracking control of flexible body switching dynamic structure

M. R. Homaeinezhad* and F. FotoohiNia

Faculty of Mechanical Engineering, K. N. Toosi University of Technology, Tehran, Iran
*Corresponding Author. E-mails: mrhomaeinezhad@kntu.ac.ir; mrh.kntu@gmail.com

Received: 19 March 2020; **Revised:** 11 May 2021; **Accepted:** 28 June 2021; **First published online:** 9 August 2021

Keywords: flexible system control; switched system control; unstructured uncertainty; multivariable control systems; sliding mode control

Abstract

In dynamically switched systems with unknown switching signal, the control system is conventionally designed based on the worst switching scenario to ensure system stability. Such conservative design demands excessive control effort in less critical switching configurations. In the case of continuum mechanics systems, such excessive control inputs result in increased structural deformations and resultant modeling uncertainties. These deformations alter differential equations of motion which cripple the task of control. In this paper, a new approach for tracking control of uncertain continuum mechanics multivariable systems undergoing switching dynamics and unknown time delay has been proposed. Control algorithm is constructed based on the mathematical rigid model of the plant and a Common Lyapunov Function (CLF) is proposed upon sliding hyperplane regarding all switching configurations. Considering the model-based nature of sliding mode control (SMC) and inevitable uncertainties induced from modeling simplifications of continuum system or parameter evaluation errors, Finite Element Analysis (FEA) is utilized to approximate total model uncertainties. To obtain robust stability, instead of conventional switching functions in the construction of control law, the control inputs are selected such that system dynamics reside within stability bounds which are calculated based on the Lyapunov asymptotic stability criterion. Therefore, the unwanted chattering issue caused by continuous switching is not observed in control input signals. Eventually, the accuracy of the proposed method has been verified through the student version of ANSYS® mechanical APDL-based simulations and its effectiveness has been demonstrated in multiple operating conditions.

1. Introduction

1.1. Overview

Continuum mechanics vibrations are capable of imposing destructive effects in the performance of control systems and generally result in closed-loop instability. Presence of model uncertainties is generally caused by either insufficient data in parameter evaluation or unmodeled dynamics [1]. Uncertain switched systems exhibit other types of model uncertainties such that governing dynamical equations alter spontaneously when switching occurs. The situation becomes critical in the case of continuum mechanics systems when unstructured uncertainties dominancy renders system response more unpredictable. Thus, it is easy to show that controller design and verification solely based on the rigid model of system would not guarantee similar performance when applied to continuum mechanics systems. In addition, analytical approaches in determining model uncertainties are not always practical due to the following reasons:

- Dynamical response of continuum mechanics system results from the superposition of infinite number of vibrational modes nevertheless, only the first few modes are generally taken into account in the construction of control algorithm to avoid burdensome calculations.

- Analytical continuous beam models like Euler–Bernoulli or Timoshenko that are utilized in the modal analysis are only valid during small deformations when the beam's radius of curvature is considered to be linearly related to vertical deformations throughout beam length [2].
- The corresponding partial differential equations solution is not attainable analytically in the presence of any form of nonlinearities such as nonlinear springs, bearings backlash, Coulomb friction.
- Control algorithm for the unknown switched system is conventionally developed considering worst switching case to guarantee stability in all switching modes. As a result, excessive control inputs would intensify system nonlinearities and corresponding unstructured uncertainties. Overwhelming inaccuracy caused by thre resence of such unmodeled dynamics would eventually result in unpredictable closed-loop response and terminal instability

Therefore, it could be inferred that rigid or even analytical flexible model of the system reflects only a portion of dynamical behaviors and accordingly the ignored dynamics would appear neither in controller design nor in simulation. Considering the aforementioned complications, the control problem of an uncertain continuum mechanics system with the unknown switching configuration constitutes the core part of the current study.

Control of uncertain switched systems has been widely studied in the existing literature. Due to inherent difficulties [3] such as maintaining system stability between switch configurations, inconsistent tracking performance, unknown frequency in which switching occurs, unknown dynamical behavior due to variable switching conditions, etc., a control algorithm capable of ensuring system stability and desirable tracking performance is not easy to achieve. Therefore, most studies are dedicated to a specific class of systems and limited conditions. For instance, Huang et al. [4] focused their studies upon finite-time output tracking for a class of switched nonlinear systems with polynomial state equations. Yang et al. [5] investigated an optimal approach regarding the class of switched linear parameter variable systems via multiple parameter-dependent Lyapunov functions. Wu et al. [6] introduced a novel controller based on backstepping method for a specific class of strict forward systems. Some researchers followed a similar framework from an adaptive point of view [7,8]. Zhang et al. investigated tracking control of linear parameter variable flexible hypersonic vehicle through H_∞ approach. However, their investigations are limited to linear systems and only parametric uncertainties are included in their framework [9]. M.R. Homaeinezhad et al. introduced an appropriate solution to the control problem corresponding to the class of parametrically uncertain systems covering unknown time delay and inaccessible switching mode detection [10]. Although the algorithm exhibits acceptable tracking performance in presence of an unknown switching signal, the proposed theory does not include unstructured uncertainties and controller performance is verified on a rigid mechanism, thus, the results cannot be generalized for continuous vibrational systems. Considering the fact that sliding mode control techniques are renowned for their robust behavior and are capable of ensuring stabilization of closed-loop systems in presence of modeling uncertainty, switched system control algorithm is constructed based on discrete sliding mode technique.

Investigations in the field of control of vibrational systems are categorized into two major fields. A group of studies address the problem of suppression of vibrations and are mainly dedicated to vibrational attenuation of a beam or flexible mechanisms using piezoelectric actuators [11–13]. Zhang et al. [14] used adaptive sliding mode in control of parallel mechanism with flexible links. The other groups are conducted prioritizing stabilization and tracking problems of flexible mechanisms with or without vibration attenuation [15,16] which is also the approach the current paper adapts. Franco et al. [17] discussed balancing control of an inverted pendulum using an energy-shaping controller with adaptive disturbance-compensation. In their investigations, analytical system modeling in the construction of control algorithm is followed and dynamical behavior is assumed to be incorporated by only the first mode shape. Chen et al. [18] proposed control of a nonlinear manipulator with Duffing oscillator dynamics and used numerical methods for solving nonlinear equations. Though being theoretically rich, the method is not easily applicable to more complicated nonlinear problems due to burdensome calculation. In recent literature regarding problem of control of vibrational systems, it has been widely accepted to

https://doi.org/10.1017/S0263574721001004 Published online by Cambridge University Press

employ FEA for defining mode shapes and natural frequencies [19]. But exploiting the idea to benefit in case of uncertainty estimation is rarely addressed. Homaeinezhad et al. [20] devised a novel approach to estimate model parametric and unstructured uncertainties by synchronizing an identical dummy model with a real system in an FEA environment. Considering high costs and space limitations usually encountered in the implementation of feedback sensors, the control algorithm is being assisted by FEA such that it only requires a limited number of sensors to approximate model uncertainties. But their investigations did not include the situation when system dynamic switches between various configurations. Following this idea, the FEA-based uncertainty estimator is used in this framework to include the effect of flexibility and unstructured uncertainties in control of switched systems.

1.2. Innovations

In order to address the aforementioned issues and overcome the existing shortcomings in available literature, this paper proposes major development over the previously presented algorithm to make it capable of controlling uncertain flexible Multi-Input Multi-Output (MIMO) systems under uncertain switching signals. This paper features the following novel contributions:

- Common Lyapunov function is proposed based on sliding hyperplane featuring every individual subsystem at given switch configuration. Therefore, the system is proven to be asymptotically stable in finite time regardless of active configuration. In case that the system is affected by an unknown time delay, Lyapunov–Krasovskii Function (LKF) is utilized instead.
- Dummy models regarding each switch configuration are constructed and run simultaneously with the real system to estimate system parametric and unstructured uncertainties.
- Controller input gain parametric uncertainties are included in the construction of control algorithm thus calculation of input bounds includes probable deviations between the real plant and rigid model.

This paper is organized as followed. Section 2 presents the problem definition and general formulation of the problem to be solved in this research. The mathematical basis required for the construction of control algorithm is proposed in Section 3. The control model for MIMO vibrational switched system has been numerically evaluated using ANSYS® simulations, the results of which are presented and analyzed in Section 4.

2. Problem Definition

In the case of rigid dynamical systems, SMC algorithm establishment is possible even for rather complicated mechanisms. However, for continuum mechanics systems, the equations of motions are often extracted based on the calculation of complicated system energy expressions such as Lagrange or Hamilton principle. The obtained equations generally include complicated terms constituting spatial derivatives resulted from transverse vibrations of continuum subsystems which render the expressions difficult to work within control applications.

In order to derive dynamical equations of motion regarding continuum mechanics system, modal analysis is required to demonstrate transverse vibrations. To this end, corresponding partial differential equations should be transformed to set of ordinary differential equations [2] using Eq. (1):

$$w\,(,t) = \sum_{j=1}^{m_\phi} \Phi_j\,(\xi)\,q_j(t) \tag{1}$$

where $w(\xi, t)$ denotes discretized expression of transverse vibration, $\Phi_j(\xi)$ are potentially unknown spatial functions regarding mode shapes in certain boundary conditions, $q_j(t)$ are corresponding temporal state variables and m_ϕ is the total number of mode shapes used for discretization of transverse vibrations.

https://doi.org/10.1017/S0263574721001004 Published online by Cambridge University Press

In order to mitigate calculation burden during discretization, only a limited number of vibrational modes are taken into account and usually, high-frequency modes are ignored due to their relatively minor effects. This approximation is not valid when the system is stimulated by high-frequency disturbances that resonate with high-frequency modes and amplify their already ignored effect. The issue demands more attention when switching occurs and alters system dynamics in an unknown pattern.

In this section, discrete form of state-space realization of MIMO continuum mechanics systems is expressed in Eq. (2). The obtained formulations are subsequently used in the construction of control algorithm. The procedure of obtaining dynamical expressions of Eq. (2) is detailed in the authors' previous work [20]. In this study, a novel control algorithm is proposed considering this class of dynamical systems under arbitrarily generated switching effects. In addition, the significant effect of control input gains uncertainty which was ignored previously will be included here. The considered class of dynamical systems without switching effects is expressed as

$$\begin{aligned} \underline{\boldsymbol{x}}_{\mathrm{r}}(k+1) &= \underline{\boldsymbol{f}}_{\boldsymbol{r}}[\underline{\boldsymbol{x}}(k)] + \mathrm{f}_{\mathrm{q}}[\underline{\boldsymbol{x}}_{q}(k)] + \boldsymbol{B}(k)\underline{\boldsymbol{u}}(k) + \underline{\boldsymbol{\nu}}(k) \\ \underline{\boldsymbol{\nu}}(k) &= [\nu_1(k),\ \cdots,\ \nu_{m_u}(k)] \\ \nu_i(k) &= \underline{\boldsymbol{b}}_{i,k-1}^{T}(k)\underline{\boldsymbol{u}}(k-1) + \cdots + \underline{\boldsymbol{b}}_{i,k-m_c}^{T}(k)\underline{\boldsymbol{u}}(k-m_c) \end{aligned} \tag{2}$$

where $\underline{\mathbf{x}}_{\mathrm{r}}(k) = [x_1(k),\ \cdots,\ x_{m_r}(k)]^{\mathrm{T}}$ denotes position vectors corresponding to rigid states and $\mathrm{m_r}$ represents system total degrees of freedom (DOF). $\mathbf{x}_{\mathrm{k}}$ denotes states corresponding to a rigid model of the system and $\underline{\mathbf{x}}_{\mathrm{q}}(\mathrm{k}) = [\underline{\mathbf{x}}(\mathrm{k}),\ \underline{\mathbf{q}}_{\mathrm{f}}(\mathrm{k})]$ includes both system states relating to rigid dynamics along with continuum mechanics vibrational terms $\mathrm{q_i(k)}$. $\underline{\boldsymbol{\nu}}(\mathrm{k})$ contains terms corresponding to past values of control inputs resulted from discretization order of $\mathrm{m_c}$. $\mathbf{f}_{\mathrm{r}}[\underline{\mathbf{x}}(\mathrm{k})]$ includes dynamical terms related to a rigid model of system and $\mathbf{f}_{\mathrm{q}}[\underline{\mathbf{x}}_{\mathrm{q}}(\mathrm{k})]$ represents dynamical effects resulted from continuum mechanics vibrations which is difficult to accurately ascertain and will be approximated in this study. $\mathbf{B}(\mathrm{k})$ denotes control input gains including both parametric and unstructured uncertainties, $\mathrm{m_u}$ is the total number of control inputs and $\underline{\mathbf{u}}(\mathrm{k})$ stands for control input vector for MIMO system.

Considering multiple switching configurations, Eq. (2) for each individual subsystem can be written like:

$$x_{r_{ij}}(k+1) = f_{r_{ij}}\left[\underline{\boldsymbol{x}}(k)\right] + f_{q_{ij}}\left[\underline{\boldsymbol{x}}_{q}(k)\right] + \underline{\boldsymbol{b}}_{ij}^{T}(k)\underline{\boldsymbol{u}}(k) + \nu_{ij}(k) \tag{3}$$

where index *j* stands for arbitrary switching configuration for each term.

In conclusion, for MIMO continuous vibrational systems, the existence of spatial derivative terms of transverse vibrations, nonlinear terms, and boundary conditions in addition to various interactions between subsystems tend to render the task of obtaining a dynamical model almost inaccessible, resource demanding, and potentially inaccurate. Naturally, dynamical and numerical analysis of obtained models is likewise impossible. The fact that few studies have been conducted to address tracking control of MIMO flexible system indicates the aforementioned issue. In this paper, overcoming complications arising from the difficulty of dynamical analysis in control of switched vibrational systems is discussed and FEA is applied to approximate modeling uncertainties caused by the continuum mechanics vibrations.

3 Main results

Considering the proposed model for each individual subsystem in Eq.(3), in this section, discrete sliding mode control (DSMC) algorithm will be developed such that closed-loop stability and tracking performance of continuum mechanics MIMO system in presence of both parametric and unstructured uncertainties with unknown switching configuration is ensured. To this end, the sliding function $\mathrm{s_{ij}(k)}$ for each individual subsystem i at given switching configuration j is defined as

$$s_{ij}(k) \triangleq \tilde{x}_{r_{ij}}(k) + \lambda_{ij}\tilde{x}_{r_{ij}}(k-1) \tag{4}$$

https://doi.org/10.1017/S0263574721001004 Published online by Cambridge University Press

Where $\tilde{x}_{r_{ij}}(k) = x_{r_{ij}}(k) - x_{id}(k)$ and $x_{id}(k)$ is the desired reference for $x_i(k)$. λ_{ij}s are control parameters set such that $s_{ij}(k) = 0$ would result in $x_{rij}(k) = x_{id}(k)$.

Remark 1 (Considerations of measurement noise). In order to involve measurement noise in the construction of proposed algorithm, two approaches are available. In the first method, stochastic characteristics of measurement noise such as probability density function type or noise probability moment are required to be precisely approximated to achieve acceptable consistency with system real measurement conditions. In addition, the variations of measurement noise statistical characteristics over system nonlinear dynamics manifold are required to be obtained. In such cases, nonlinear filters such as cubature or unscented Kalman filters are utilized in which statistical variables of the stochastic process are being updated continuously via sigma points. However, statistical characteristic of this measurement noise generally cannot be classified as stationary white noises rendering complications in certain circumstances [21]. As another approach, one would suggest using analogue low-pass filters to remove measurement noise in the construction of control scheme. Since the filter is considered to be analogue, phase shift and amplitude distortion relative to those of the original signal are neglectable. Hence, the influence of filtering could be considered in feedback control through the incorporation of filter dynamics in control calculations according to Eq. (5).

$$\hat{s}_{ij}(k) = \frac{2 - \omega_{0s}T}{2 + \omega_{0s}T}\hat{s}_{ij}\,(k-1) + \frac{\omega_{0s}T}{2 + \omega_{0s}T}\left[s_{ij}(k) + s_{ij}\,(k-1)\right] \tag{5}$$

In addition, high-frequency signals included in control inputs that are generated due to measurement noise are normally ignored due to the limited frequency bandwidth of physical actuators. In other words, physical actuator dynamics oftentimes behave as a first-order low-pass filter in the presence of high-frequency signals. In such cases, it is necessary to similarly incorporate actuator dynamics in the construction of control law.

$$u_i(k) = \frac{2 - \omega_{0a}T}{2 + \omega_{0a}T}u_i\,(k-1) + \frac{\omega_{0a}T}{2 + \omega_{0a}T}\left[u_{ic}(k) + u_{ic}\,(k-1)\right] \tag{6}$$

In Eqs. (5), and (6), ω_{0s} and ω_{0a} are bandwidth frequencies corresponding to low-pass filters applied, respectively, to sliding functions and control input signals. Replacing $u_i(k)$ from Eq. (6) into convex inequality of Eq. (14) which is being discussed further, $\underline{U}_c(K-1) = [U_{1c}(k), \cdots U_{nc}(k)]^T$ is obtained. Hence, the control signal is calculated considering actuators' frequency bandwidth and measurement noise effects [15].

Remark 2 (Sliding functions parameter). It can be shown that setting $|\lambda_{ij}| < 1$ drives individual system states to desired references if $s_{ij}(k) = 0$.

Assumption 1. *The system is considered to be in squared format for simplicity purposes in obtaining the control model, that is, the controller gain matrix is square and invertible. In such cases, sliding functions are assigned to those DOFs that correspond to a tracking objective.*

Substituting $x_{rij}(k)$ from Eq. (3) into Eq. (4) and shifting the equation for one sample ahead results in:

$$s_{ij}\,(k+1) = f_{r_{ij}}\left[\underline{\boldsymbol{x}}(k)\right] + f_{q_{ij}}\left[\underline{\boldsymbol{x}}_q(k)\right] + v_{ij}(k) + \lambda_{ij}x_{rij}(k) - x_{id}\,(k+1) - \lambda_{ij}x_{id}(k) + \underline{\boldsymbol{b}}_{ij}^T(k)\underline{\boldsymbol{u}}(k) \tag{7}$$

Eq. (7) is further summarized to Eq. (8):

$$\begin{aligned} s_{ij}(k+1) &= f_{rij}[\underline{\mathbf{x}}(k)] + f_{q_{ij}}[\underline{\mathbf{x}}_q(k)] + \underline{b}_{ij}^T(k)\underline{u}(k) + v_{ij}(k) + \xi_{ij}(k), \\ \xi_{ij}(k) &\triangleq \lambda_{ij}x_{rij}(k) - x_{id}\,(k+1) - \lambda_{ij}x_{id}(k) \end{aligned} \tag{8}$$

https://doi.org/10.1017/S0263574721001004 Published online by Cambridge University Press

Theorem 1. *Discrete-Time MIMO flexible system response expressed in Eq. (2) under unknown switching signal and both parametric and unstructured uncertainties will follow the desired sliding set* $\boldsymbol{\Omega_i} = \{s_i(k) : |s_i(k)| \leq \rho_i\}$ *in finite number of samples under Assumption 1. In case control input is selected within calculated bounds, it is as follows:*

$$\underline{\boldsymbol{u}}(k) = [1 - \alpha(k)]\, \boldsymbol{B}^{-1}(k)\underline{\boldsymbol{Q}}_L(k) + \alpha(k)\boldsymbol{B}^{-1}(k)\underline{\boldsymbol{Q}}_H(k)$$
$$\alpha(k) \in (0, 1) \tag{9}$$

$\underline{\mathbf{Q}}_{\mathrm{L}}(\mathrm{k})$ and $\underline{\mathbf{Q}}_{\mathrm{H}}(\mathrm{k})$ are calculated as lower and upper control input bounds and $\alpha(\mathrm{k})$ is the control input proximity factor which is set by the control designer.

Proof. Candidate Lyapunov function $\mathrm{V_i(k)}$ for each subsystem is defined in Eq. (10).

$$V_i(k) \triangleq \left[\sum_{j=1}^{m_\sigma} \eta_{ij} s_{ij}(k)\right]^2 \tag{10}$$

In Eq. (10), m_σ is the number of total possible switching configurations and $\eta_{\mathrm{ij}} > 0$ is an arbitrary weighting factor set by the designer in accordance with the possibility and severity of each switching configuration. The control law corresponding to the dynamical model presented in Eq. (2) is derived such that candidate Lyapunov function is monotonically decreasing. In order to attain finite-time convergence, the Lyapunov function should satisfy Eq. (11) with finite-time convergence factor of $\mu_{\mathrm{i}} \in (0, 1)$

$$V_i\,(k+1) < \mu_i^2 V_i(k) \tag{11}$$

As a result;

$$\left[\sum_{j=1}^{m_\sigma} \eta_{ij} s_{ij}\,(k+1)\right]^2 < \mu_i^2 \left[\sum_{j=1}^{m_\sigma} \eta_{ij} s_{ij}(k)\right]^2 \tag{12}$$

Thus,

$$-\mu \left|\sum_{j=1}^{m_\sigma} \eta_{ij} s_{ij}(k)\right| < \sum_{j=1}^{m_\sigma} \eta_{ij} s_{ij}\,(k+1) < +\mu_i \left|\sum_{j=1}^{m_\sigma} \eta_{ij} s_{ij}(k)\right| \tag{13}$$

Substituting $\mathrm{s_{ij}(k+1)}$ from Eq. (8) to Eq. (13) leads to:

$$-\mu \left|\sum_{j=1}^{m_\sigma} \eta_{ij} s_{ij}(k)\right| < \sum_{j=1}^{m_\sigma} \eta_{ij} \left\{f_{r_{ij}}\left[\underline{\boldsymbol{x}}(k)\right] + f_{q_{ij}}\left[\underline{\boldsymbol{x}}_q(k)\right] + \underline{\boldsymbol{b}}_{ij}^T(k)\underline{\boldsymbol{u}}(k) + \nu_{ij}(k) + \xi_{ij}(k)\right\}$$
$$< +\mu_i \left|\sum_{j=1}^{m_\sigma} \eta_{ij} s_{ij}(k)\right| \tag{14}$$

Since real system parameters are oftentimes difficult or even impossible to accurately ascertain, parametric uncertainties are inevitable in dynamical analysis and should be considered when obtaining the control algorithm. Therefore, the nominal value of system parameters should be used in the construction of control algorithm. Defining $\mathrm{g_{ij}(k)} \triangleq \mathrm{f_{rij}[\underline{x}(k)]} + \nu_{\mathrm{ij}}(\mathrm{k})$ and $\hat{g}_{\mathrm{ij}}(\mathrm{k})$ and $\hat{f}_{\mathrm{qij}}[\underline{\mathbf{x}}_{\mathrm{q}}(\mathrm{k})]$ as approximations (with known nominal parameters) of rigid model and flexible terms, respectively, Eq. (14) turns to Eq. (15) by adding and subtracting the approximated terms $\hat{\mathrm{g}}_{\mathrm{ij}}(\mathrm{k}) + \hat{\mathrm{f}}_{\mathrm{qij}}[\underline{\mathbf{x}}_{\mathrm{q}}(\mathrm{k})]$.

$$-\mu \left|\sum_{j=1}^{m_\sigma} \eta_{ij} s_{ij}(k)\right| < \sum_{j=1}^{m_\sigma} \eta_{ij} \left\{ \left[g_{ij}(k) + f_{q_{ij}}\left[\underline{\boldsymbol{x}}_q(k)\right]\right] - \left[\hat{g}_{ij}(k) + \hat{f}_{q_{ij}}\left[\underline{\boldsymbol{x}}_q(k)\right]\right] + \hat{g}_{ij}(k)\right.$$
$$\left. + \hat{f}_{q_{ij}}\left[\underline{\boldsymbol{x}}_q(k)\right] + \underline{\boldsymbol{b}}_{ij}^T(k)\underline{\boldsymbol{u}}(k) + \xi_{ij}(k)\right\} < +\mu_i \left|\sum_{j=1}^{m_\sigma} \eta_{ij} s_{ij}(k)\right| \tag{15}$$

https://doi.org/10.1017/S0263574721001004 Published online by Cambridge University Press

By subtracting $\sum_{j=1}^{m_\sigma} \eta_{ij}\{[g_{ij}(k)+f_{q_{ij}}[\underline{x}_q(k)]]-[\hat{g}_{ij}(k)+\hat{f}_{q_{ij}}[\underline{x}_q(k)]]+\hat{g}_{ij}(k)+\hat{f}_{q_{ij}}[\underline{x}_q(k)]+\xi_{ij}(k)\}$ from all sides of convex inequality of (15), it is obtained that:

$$
\begin{aligned}
&-\sum_{j=1}^{m_\sigma}\eta_{ij}\left\{\left[g_{ij}(k)+f_{q_{ij}}\left[\underline{x}_q(k)\right]\right]-\left[\widehat{g}_{ij}(k)+\widehat{f}_{q_{ij}}\left[\underline{x}_q(k)\right]\right]+\widehat{g}_{ij}(k)+\widehat{f}_{q_{ij}}\left[\underline{x}_q(k)\right]+\xi_{ij}(k)\right\}\\
&-\mu_i\left|\sum_{j=1}^{m_\sigma}\eta_{ij}s_{ij}(k)\right|<\sum_{j=1}^{m_\sigma}\eta_{ij}\left[\underline{b}_{ij}^{T}(k)\underline{u}(k)\right]<-\sum_{j=1}^{m_\sigma}\eta_{ij}\left\{\left[g_{ij}(k)+f_{q_{ij}}\left[\underline{x}_q(k)\right]\right]\right.\\
&\left.-\left[\widehat{g}_{ij}(k)+\widehat{f}_{q_{ij}}\left[\underline{x}_q(k)\right]\right]+\widehat{g}_{ij}(k)+\widehat{f}_{q_{ij}}\left[\underline{x}_q(k)\right]+\xi_{ij}(k)\right\}+\mu_i\left|\sum_{j=1}^{m_\sigma}\eta_{ij}s_{ij}(k)\right|
\end{aligned}
\tag{16}
$$

Remark 3 (Uncertainty estimation). The term $[g_{ij}(k)+f_{q_{ij}}[\underline{x}_q(k)]]-[\hat{g}_{ij}(k)+\hat{f}_{q_{ij}}[\underline{x}_q(k)]]$ and $\hat{f}_{qij}[\underline{x}_q(x)]$ respectively, express parametric and unstructured uncertainties of the vibrational system for any given switching configuration. At this state, FEA dummy models are generated corresponding to each specific switching configuration. Since dummy models are analyzed in the FEA framework using an adequate number of elements, dynamical responses actually include the influence of high-frequency modes and could potentially represent real system's behavior. Thus it can be inferred that any dynamical responses deviation in comparison with the real system is related to parametric evaluation errors. This approximation generally holds true due to the FEA capability in modeling vibrational modes. Similarly, unstructured uncertainties could be obtained comparing dynamical behavior of dummy models and mathematical rigid model of the system. It should be noted that one-step lagged approximation is inevitable due to limited data availability at the current time step.

$$
\begin{aligned}
g_i(k)+f_{qij}[\underline{x}_q(k)] &\approx x_{rij}(k)-\underline{b}_{ij}^{T}(k)\underline{u}(k)\\
\hat{f}_{qij}[\underline{x}_q(k)] &\approx \hat{x}_{rij}(k)-\underline{b}_{ij}^{T}(k)\underline{u}(k)-\hat{g}_{ij}(k)
\end{aligned}
\tag{17}
$$

System states for dummy models are expressed as $\hat{x}_{ij}(k)$ at given switching configuration of j. Considering approximations in Eq. (17), Eq. (16) yield to Eq.(18):

$$
\begin{aligned}
&-\sum_{j=1}^{m_\sigma}\eta_{ij}\left\{x_{rij}(k)-\widehat{x}_{r_{ij}}(k)+\widehat{g}_{ij}(k)+\widehat{f}_{q_{ij}}\left[\underline{x}_q(k)\right]+\xi_{ij}(k)\right\}\\
&-\sum_{j=1}^{m_\sigma}\eta_{ij}\left\{-\left[\underline{b}_{ij}^{T}(k-1)-\hat{\underline{b}}_{ij}^{T}(k-1)\right]\underline{u}(k-1)\right\}-\mu_i\left|\sum_{j=1}^{m_\sigma}\eta_{ij}s_{ij}(k)\right|\\
&<\sum_{j=1}^{m_\sigma}\eta_{ij}\left[\underline{b}_{ij}^{T}(k)\underline{u}(k)\right]<+\mu_i\left|\sum_{j=1}^{m_\sigma}\eta_{ij}s_{ij}(k)\right|-\sum_{j=1}^{m_\sigma}\eta_{ij}\left\{-\left[\underline{b}_{ij}^{T}(k-1)-\hat{\underline{b}}_{ij}^{T}(k-1)\right]\underline{u}(k-1)\right\}\\
&-\sum_{j=1}^{m_\sigma}\eta_{ij}\left\{x_{r_{ij}}(k)-\widehat{x}_{r_{ij}}(k)+\widehat{g}_{ij}(k)+\widehat{f}_{q_{ij}}\left[\underline{x}_q(k)\right]+\xi_{ij}(k)\right\}
\end{aligned}
\tag{18}
$$

Assumption 2. *The matrix* $\mathbf{B}_j(k)\triangleq\begin{bmatrix}\mathbf{B}_{1j}^{T}(k)\\ \vdots\\ \mathbf{B}_{m_xj}^{T}(k)\end{bmatrix}$, $\mathbf{B}_j(k)\in\mathbb{R}^{m_x\times m_x}$ *expressing control signal multipliers for total* m_x *subsystems and given switching signal j is considered to include multiplicative uncertainty.* $\boldsymbol{B}_j(k)$*is therefore expressed as in Eq. (19).* □

$$
\mathbf{B}_j(k)\triangleq\left[\mathbf{I}+\mathbf{\Gamma}_j(k)\right]\hat{\mathbf{B}}_j(k)
\tag{19}
$$

https://doi.org/10.1017/S0263574721001004 Published online by Cambridge University Press

In which $\mathbf{\Gamma}_j(k)$ denotes the uncertainty matrix with known bounds and $\hat{\mathbf{B}}_j(k)$ is the approximated controller signal multiplier matrix with nominal parameters. Furthermore, it is assumed that $\mathbf{B}_j(k)\mathbf{\Gamma}_j(k)$ is nonsingular for all possible cases of model uncertainty and switching signals.

The terms at the sides of inequality expressed in Eq. (18) determine stability bounds of a control input signal in the form of $q_{l,i}(k) \le \sum_{j=1}^{m\sigma} \eta_{ij}[\underline{\mathbf{b}}_{ij}^{T}(k)\underline{\mathbf{u}}(k)] \le q_{h,i}(k)$ for every individual subsystem considering all switching signals j in which $q_{l,i}(k)$ and $q_{h,i}(k)$ denote lower and upper stability bounds, respectively. Similar expressions could be obtained for all rigid dynamical states $i = 1, \ldots, m_r$ therefore, the terms corresponding to control inputs bounds are merged into a set of convex inequalities according to Assumption 2.

$$\underline{\mathbf{q}}_L(k) < \left\{ \sum_{j=1}^{m_\sigma} \begin{bmatrix} \eta_{1j} & \cdots & 0 \\ \vdots & \ddots & \vdots \\ 0 & \cdots & \eta_{m_x,j} \end{bmatrix} \left[\mathbf{B}_j(k)\right] \right\} \underline{\mathbf{u}}(k) < \underline{\mathbf{q}}_H(k) \tag{20}$$

Where $\underline{\mathbf{q}}_L(k) = [q_{l,1}(k) \ \cdots \ q_{l,m_u}(k)]^T$ and $\underline{\mathbf{q}}_H(k) = [q_{h,1}(k) \ \cdots \ q_{h,m_u}(k)]^T$.

According to Assumption 2, control input gains uncertainties equation $[\mathbf{B}_j(k-1) - \hat{\mathbf{B}}_j(k-1)] = \mathbf{\Gamma}_j(k-1)\hat{\mathbf{B}}_j(k-1)$ is obtained. Adapting the introduced format in Eq. (20), stability bounds on either side of Eq. (18) could be rewritten as Eqs. (21–22) such that they include all subsystems.

$$\begin{aligned} \underline{\mathbf{q}}_L(k) \triangleq & \left\{ \sum_{j=1}^{m_\sigma} \begin{bmatrix} \eta_{1j} & \cdots & 0 \\ \vdots & \ddots & \vdots \\ 0 & \cdots & \eta_{m_x,j} \end{bmatrix} \left[\mathbf{\Gamma}_j(k-1)\widehat{\mathbf{B}}_j(k-1)\right] \right\} \underline{\mathbf{u}}(k-1) \\ & + \begin{bmatrix} -\sum_{j=1}^{m_\sigma} \eta_1^j \left\{ x_{r_i}^j(k) - \widehat{x}_{r_i}j(k) + \widehat{g}_{1j}(k) + \widehat{f}_{q_{1j}}\left[\underline{\mathbf{x}}_q(k)\right] + \xi_{1j}(k) \right\} - \mu_1 \left| \sum_{j=1}^{m_\sigma} \eta_{1j} s_{1j}(k) \right| \\ \vdots \\ -\sum_{j=1}^{m_\sigma} \eta_{m_x j} \left\{ x_{m_x j}(k) - \widehat{x}_{m_x j}(k) + \widehat{g}_{m_x j}(k) + \widehat{f}_{q_{m_x j}}\left[\underline{\mathbf{x}}_q(k)\right] + \xi_{m_x j}(k) \right\} - \mu_{m_x} \left| \sum_{j=1}^{m_\sigma} \eta_{m_x,j} s_{m_x,j}(k) \right| \end{bmatrix} \end{aligned} \tag{21}$$

$$\begin{aligned} \underline{\mathbf{q}}_H(k) \triangleq & \\ & \times \begin{bmatrix} -\sum_{j=1}^{m_\sigma} \eta_{1j} \left\{ x_{r_{ij}}(k) - \widehat{x}_{r_{ij}}(k) + \widehat{g}_{1j}(k) + \widehat{f}_{q_{1j}}\left[\underline{\mathbf{x}}_q(k)\right] + \xi_{1j}(k) \right\} + \mu_1 \left| \sum_{j=1}^{m_\sigma} \eta_{1j} s_{1j}(k) \right| \\ \vdots \\ -\sum_{j=1}^{m_\sigma} \eta_{m_x j} \left\{ x_{m_x j}(k) - \widehat{x}_{m_x j}(k) + \widehat{g}_{m_x j}(k) + \widehat{f}_{q_{m_x j}}\left[\underline{\mathbf{x}}_q(k)\right] + \xi_{m_x j}(k) \right\} + \mu_{m_x} \left| \sum_{j=1}^{m_\sigma} \eta_{m_x,j} s_{m_x,j}(k) \right| \end{bmatrix} \\ & + \left\{ \sum_{j=1}^{m_\sigma} \begin{bmatrix} \eta_{1j} & \cdots & 0 \\ \vdots & \ddots & \vdots \\ 0 & \cdots & \eta_{m_x,j} \end{bmatrix} \left[\mathbf{\Gamma}_j(k-1)\widehat{\mathbf{B}}_j(k-1)\right] \right\} \underline{\mathbf{u}}(k-1) \end{aligned} \tag{22}$$

Then, using $0 < \alpha(k) < 1$ as proximity factor, control signals are obtained as

$$\underline{\mathbf{u}}(k) = [1 - \alpha(k)]\,\mathbf{B}^{-1}(k)\underline{\mathbf{Q}}_L(k) + \alpha(k)\mathbf{B}^{-1}(k)\underline{\mathbf{Q}}_H(k)$$

https://doi.org/10.1017/S0263574721001004 Published online by Cambridge University Press

$$\underline{\mathbf{Q}}_L(\mathrm{k}) = \left\{ \sum_{\mathrm{j}=1}^{\mathrm{m}_\sigma} \begin{bmatrix} \eta_{1\mathrm{j}} & \cdots & 0 \\ \vdots & \ddots & \vdots \\ 0 & \cdots & \eta_{\mathrm{m_x,j}} \end{bmatrix} \left[\mathbf{I} + \mathbf{\Gamma}_\mathrm{j}(\mathrm{k})\right] \hat{\mathbf{B}}_\mathrm{j}(\mathrm{k}) \right\}^{-1} \underline{\mathbf{q}}_\mathrm{L}(\mathrm{k})$$

$$\underline{\mathbf{Q}}_\mathrm{H}(\mathrm{k}) = \left\{ \sum_{\mathrm{j}=1}^{\mathrm{m}_\sigma} \begin{bmatrix} \eta_{1\mathrm{j}} & \cdots & 0 \\ \vdots & \ddots & \vdots \\ 0 & \cdots & \eta_{\mathrm{m_x,j}} \end{bmatrix} \left[\mathbf{I} + \mathbf{\Gamma}_\mathrm{j}(\mathrm{k})\right] \hat{\mathbf{B}}_\mathrm{j}(\mathrm{k}) \right\}^{-1} \underline{\mathbf{q}}_\mathrm{H}(\mathrm{k}) \tag{23}$$

Proof of Theorem 1 ends here.

Proposition 1 (Consideration of time delay). *In case the system dynamics is being affected by time delay, the dynamical equations of motion and corresponding sliding functions should be modified accordingly. To this end, the dynamical discrete model Eq. (3) should include terms corresponding to the effect of time delay. In order to consider the difficulty of locating the exact point in which time delay affects system dynamic, the time delay is considered unknown with limited bounds such that* $m_{d,ij} \in \left[1, \bar{m}_{dij}\right]$ *where* $\bar{m}_{dij}$ *is the maximum delay corresponding to individual subsystem i at given switching configuration of j. The procedure of obtaining a control algorithm in the presence of time delay is briefly discussed as followed.*

$$\begin{aligned} \mathrm{x}_{\mathrm{rij}}(\mathrm{k}+1) = {} & \mathrm{f}_{\mathrm{rij}}\left[\underline{\mathbf{x}}(\mathrm{k})\right] + \mathrm{f}_{\mathrm{qij}}\left[\underline{\mathbf{x}}_\mathrm{q}(\mathrm{k})\right] + \mathrm{h}_{\mathrm{rij}}\left[\underline{\mathbf{x}}\left(\mathrm{k}-\mathrm{m}_{\mathrm{d,ij}}\right)\right] + \mathrm{h}_{\mathrm{qij}}\left[\underline{\mathbf{x}}_\mathrm{q}\left(\mathrm{k}-\mathrm{m}_{\mathrm{d,ij}}\right)\right] \\ & + \underline{\mathbf{b}}_{\mathrm{ij}}^{\mathrm{T}}(\mathrm{k})\underline{\mathbf{u}}(\mathrm{k}) + \nu_{\mathrm{ij}}(\mathrm{k}) \end{aligned} \tag{24}$$

In Eq. (24), $\mathrm{h}_{\mathrm{rij}}, \mathrm{h}_{\mathrm{qij}}:\mathbb{R}^{\mathrm{m_x}} \to \mathbb{R}$ are switched functions corresponding to sections of system dynamics that include time delay. Consequently, sliding functions Eq. (8) are required to be rewritten as Eq. (25).

$$\begin{aligned} \mathrm{s}_{\mathrm{ij}}(\mathrm{k}+1) = {} & \mathrm{f}_{\mathrm{rij}}\left[\underline{\mathbf{x}}(\mathrm{k})\right] + \mathrm{f}_{\mathrm{q_{ij}}}\left[\underline{\mathbf{x}}_\mathrm{q}(\mathrm{k})\right] + \mathrm{h}_{\mathrm{rij}}\left[\underline{\mathbf{x}}\left(\mathrm{k}-\mathrm{m}_{\mathrm{d,ij}}\right)\right] + \mathrm{h}_{\mathrm{q_{ij}}}\left[\underline{\mathbf{x}}_\mathrm{q}\left(\mathrm{k}-\mathrm{m}_{\mathrm{d,ij}}\right)\right] \\ & + \underline{\mathrm{b}}_{\mathrm{ij}}^{\mathrm{T}}(\mathrm{k})\underline{\mathrm{u}}(\mathrm{k}) + \nu_{\mathrm{ij}}(\mathrm{k}) + \xi_{\mathrm{ij}}(\mathrm{k}) \end{aligned} \tag{25}$$

In addition, the candidate Lyapunov function introduced in theorem 1 is replaced by Lyapunov–Krasovskii function (LKF) including sliding functions correspond to the effect of time delay.

$$\mathrm{V}_\mathrm{i}(\mathrm{k}) \triangleq \left[\sum_{\mathrm{j}=1}^{\mathrm{m}_\sigma} \eta_{\mathrm{ij}}\mathrm{s}_{\mathrm{ij}}(\mathrm{k})\right]^2 + \sum_{\mathrm{j}=1}^{\mathrm{m}_\sigma} \sum_{\mathrm{l}=\mathrm{k}-\mathrm{m}_{\mathrm{d,ij}}}^{\mathrm{k}-1} \beta_{\mathrm{ij}}\mathrm{s}_{\mathrm{ij}}^2(\mathrm{l}) \tag{26}$$

In Eq. (26), η_{ij} and β_{ij} are design parameters, respectively. assigned to current sliding functions and the sliding functions defined over the uncertain time delay horizon. Similar to the procedure followed in Theorem 1, to ensure attaining a monotonically decreasing LKF and attaining finite-time convergence, it is considered that $\mathrm{V}_\mathrm{i}(\mathrm{k}+1) - \mathrm{V}_\mathrm{i}(\mathrm{k}) < 0$.

$$\begin{aligned} & \mathrm{V}_\mathrm{i}(\mathrm{k}+1) - \mathrm{V}_\mathrm{i}(\mathrm{k}) < 0 \\ & \Rightarrow \left[\sum_{\mathrm{j}=1}^{\mathrm{m}_\sigma} \eta_{\mathrm{ij}}\mathrm{s}_{\mathrm{ij}}(\mathrm{k}+1)\right]^2 + \sum_{\mathrm{j}=1}^{\mathrm{m}_\sigma} \sum_{\mathrm{l}=\mathrm{k}-\mathrm{m}_{\mathrm{d,ij}}+1}^{\mathrm{k}} \beta_{\mathrm{ij}}\mathrm{s}_{\mathrm{ij}}^2(\mathrm{l}) - \left[\sum_{\mathrm{j}=1}^{\mathrm{m}_\sigma} \eta_{\mathrm{ij}}\mathrm{s}_{\mathrm{ij}}(\mathrm{k})\right]^2 - \sum_{\mathrm{j}=1}^{\mathrm{m}_\sigma} \sum_{\mathrm{l}=\mathrm{k}-\mathrm{m}_{\mathrm{d,ij}}}^{\mathrm{k}-1} \beta_{\mathrm{ij}}\mathrm{s}_{\mathrm{ij}}^2(\mathrm{l}) < 0 \end{aligned} \tag{27}$$

Design parameters η_{ij} and β_{ij} should be allocated such that $\left[\sum_{\mathrm{j}=1}^{\mathrm{m}_\sigma} \eta_{\mathrm{ij}}\mathrm{s}_{\mathrm{ij}}(\mathrm{k})\right]^2 - \sum_{\mathrm{j}=1}^{\mathrm{m}_\sigma} \beta_{\mathrm{ij}} \left[\mathrm{s}_{\mathrm{ij}}^2(\mathrm{k}) - \mathrm{s}_{\mathrm{ij}}^2\left(\mathrm{k}-\mathrm{m}_{\mathrm{d,ij}}\right)\right] > 0$. Hence, the conditions for Krasovskii weights are expressed through investigations over the term $\mathcal{P}_\mathrm{i}^2(\mathrm{k}) \triangleq \left[\sum_{\mathrm{j}=1}^{\mathrm{m}_\sigma} \eta_{\mathrm{ij}}\mathrm{s}_{\mathrm{ij}}(\mathrm{k})\right]^2 - \sum_{\mathrm{j}=1}^{\mathrm{m}_\sigma} \beta_{\mathrm{ij}} \left[\mathrm{s}_{\mathrm{ij}}^2(\mathrm{k}) - \mathrm{s}_{\mathrm{ij}}^2\left(\mathrm{k}-\mathrm{m}_{\mathrm{d,ij}}\right)\right]$ which is required to be positive.

$$\mathcal{P}_\mathrm{i}^2(\mathrm{k}) > \bar{\mathcal{P}}_\mathrm{i}^2(\mathrm{k}) \triangleq \sum_{\mathrm{j}=1}^{\mathrm{m}_\sigma} \eta_{\mathrm{ij}}^2\mathrm{s}_{\mathrm{ij}}^2(\mathrm{k}) + \sum_{\mathrm{j}=1}^{\mathrm{m}_\sigma} \sum_{\mathrm{l}=1}^{\mathrm{m}_\sigma} \eta_{\mathrm{ij}}\eta_{\mathrm{il}}\mathrm{s}_{\mathrm{ij}}(\mathrm{k})\mathrm{s}_{\mathrm{il}}(\mathrm{k}) - \sum_{\mathrm{j}=1}^{\mathrm{m}_\sigma} \beta_{\mathrm{ij}}\mathrm{s}_{\mathrm{ij}}^2(\mathrm{k}) \tag{28}$$

https://doi.org/10.1017/S0263574721001004 Published online by Cambridge University Press

A sufficient condition for $\bar{\mathcal{P}}_i^2(k) \geq 0$ can be expressed as

$$\eta_{ij}^2 s_{ij}^2(k) + \sum_{l=1}^{m_\sigma} \eta_{ij}\eta_{il} s_{ij}(k) s_{il}(k) - \beta_{ij} s_{ij}^2(k) > 0; j = 1, \ldots, .m_\sigma \tag{29}$$

Then, the feasibility conditions for Krasovkii weights are obtained as

$$\beta_{ij} < \eta_{ij}^2 + \eta_{ij} \frac{\sum_{j=1}^{m_\sigma} \eta_{il} s_{il}(k)}{s_{ij}(k)} \tag{30}$$

More details are left to be seen in [22]. Proposition 1 ends here.

Proposition 2 (Finite-time convergence). *In order to ensure closed-loop response convergence to sliding surface in finite number of steps,* $|\sum_{j=1}^{m_\sigma} \eta_{ij} s_{ij}(k+1)| < \mu_i |\sum_{j=1}^{m_\sigma} \eta_{ij} s_{ij}(k)|$ *was defined as Lyapunov asymptotic stability condition with* μ_i *as finite-time convergence factor. Therefore;*

$$\begin{aligned} &\left|\eta_{i1} s_{i1}(1) + \eta_{i2} s_{i2}(1) + \cdots + \eta_{im_\sigma} s_{im_\sigma}(1)\right| < \mu_i \left|\eta_{i1} s_{i1}(0) + \eta_{i2} s_{i2}(0) + \cdots + \eta_{im_\sigma} s_{im_\sigma}(0)\right| \\ &\Rightarrow \left|\eta_{i1} s_{i1}(2) + \eta_{i2} s_{i2}(2) + \cdots + \eta_{im_\sigma} s_{im_\sigma}(2)\right| < \mu_i \left|\eta_{i1} s_{i1}(1) + \eta_{i2} s_{i2}(1) + \cdots + \eta_{im_\sigma} s_{im_\sigma}(1)\right| \\ &< \mu_i^2 \left|\eta_{i1} s_{i1}(0) + \eta_{i2} s_{i2}(0) + \cdots + \eta_{im_\sigma} s_{im_\sigma}(0)\right| \Rightarrow \cdots \Rightarrow \left|\eta_{i1} s_{i1}(k) + \eta_{i2} s_{i2}(k) + \cdots + \eta_{im_\sigma} s_{im_\sigma}(k)\right| \\ &< \mu_i^k \left|\eta_{i1} s_{i1}(0) + \eta_{i2} s_{i2}(0) + \cdots + \eta_{im_\sigma} s_{im_\sigma}(0)\right| \end{aligned} \tag{31}$$

Sliding set is defined as $\boldsymbol{\Omega}_i = \{s_{ij}(k): \left|\sum_{j=1}^{m_\sigma} \eta_{ij} s_{ij}(k)\right| \leq \rho_i\}$. In which, $\rho_i > 0$ is half the width of the sliding band. Solving the equation $\mu_i^k \left|\eta_{i1} s_{i1}(0) + \eta_{i2} s_{i2}(0) + \cdots + \eta_{im_\sigma} s_{im_\sigma}(0)\right| = \rho_i$ for k, it is concluded that system response trajectory converges to $\boldsymbol{\Omega}_i$ in $n_{\Omega i} = \log_{\mu_i}\left(\frac{\rho_i}{\left|\eta_{i1} s_{i1}(0) + \eta_{i2} s_{i2}(0) + \cdots + \eta_{im_\sigma} s_{im_\sigma}(0)\right|}\right)$ samples.

Remark 4 (Switching dwell time). It should be noted that switching dwell time needs to be greater than convergence time calculated in Proposition 2, otherwise switching may occur before the system converges to sliding manifold resulting in closed-loop instability.

Remark 5 (Convergence to sliding hyperplane). Theorem 1 does not impose any particular value for $\eta_{ij} > 0$ in obtaining control input of Eq. (23). As a result, given multiple values of $\eta_{ij} > 0$, for a particular switching signal and a specific subsystem, theorem 1 should hold true. In case tends to zero, $|\sum_{j=1}^{m_\sigma} \eta_{ij} s_{ij}(k)| = 0$ constitute homogenous systems of equations for each individual subsystem with multiple arbitrary (not necessarily zero) η_{ij}. Thus it can be inferred that all $s_{ij}(k)$ will tend to zero for it is the only answer to each homogenous system of equations.

Proposition 3 (Sliding mode). *When the closed-loop system enters sliding manifold neighborhood with radius of* ρ_i*, that is,* $|\sum_{j=1}^{m_\sigma} \eta_{ij} s_{ij}(k)| < \rho_i$*, the stability conditions will be slightly different from Eq. (12) for reaching mode. In fact, the ideal control input should be obtained such that it forces the system dynamics to reside within sliding band.*

$$\left[\sum_{j=1}^{m_\sigma} \eta_{ij} s_{ij}(k+1)\right]^2 < \rho_i^2 \tag{32}$$

Following the procedure similar to the proof of Theorem 1, it is obtained that:

$$\underline{\boldsymbol{q}}_{\mathbf{L}}(k) < \left\{\sum_{j=1}^{m_\sigma} \begin{bmatrix} \eta_{1j} & \cdots & 0 \\ \vdots & \ddots & \vdots \\ 0 & \cdots & \eta_{m_x,j} \end{bmatrix} \left[\mathbf{I} + \boldsymbol{\Gamma}_j(k)\right] \hat{\mathbf{B}}_j(k)\right\} \underline{\mathbf{u}}(k) < \underline{\boldsymbol{q}}_{\mathbf{H}}(k) \tag{33}$$

https://doi.org/10.1017/S0263574721001004 Published online by Cambridge University Press

where $\underline{\mathbf{q}}_{(}\mathrm{k})$ and $\underline{\mathbf{q}}_{H}(\mathrm{k})$ are defined as boundary dynamical terms in sliding mode.

$$\underline{\boldsymbol{q}}_{\mathrm{L}}(\mathrm{k}) \triangleq \left\{ \sum_{\mathrm{j}=1}^{\mathrm{m}_\sigma} \begin{bmatrix} \eta_{1\mathrm{j}} & \cdots & 0 \\ \vdots & \ddots & \vdots \\ 0 & \cdots & \eta_{\mathrm{m_x,j}} \end{bmatrix} \left[\boldsymbol{\Gamma}_{\mathrm{j}}(\mathrm{k}-1) \widehat{\mathbf{B}}_{\mathrm{j}}\,(\mathrm{k}-1) \right] \right\} \underline{\mathbf{u}}\,(\mathrm{k}-1) + \begin{bmatrix} -\sum_{\mathrm{j}=1}^{\mathrm{m}_\sigma} \eta_{1\mathrm{j}} \left\{ \mathrm{x}_{\mathrm{r}1\mathrm{j}}(\mathrm{k}) - \widehat{\mathrm{x}}_{\mathrm{r}1\mathrm{j}}(\mathrm{k}) + \widehat{\mathrm{g}}_{1\mathrm{j}}(\mathrm{k}) + \widehat{\mathrm{f}}_{\mathrm{q}_{1\mathrm{j}}}\left[\underline{\mathbf{x}}_{\mathrm{q}}(\mathrm{k})\right] + \xi_{1\mathrm{j}}(\mathrm{k}) \right\} - \rho_i \\ \vdots \\ -\sum_{\mathrm{j}=1}^{\mathrm{m}_\sigma} \eta_{\mathrm{m_xj}} \left\{ \mathrm{x}_{\mathrm{m_xj}}(\mathrm{k}) - \widehat{\mathrm{x}}_{\mathrm{m_xj}}(\mathrm{k}) + \widehat{\mathrm{g}}_{\mathrm{m_xj}}(\mathrm{k}) + \widehat{\mathrm{f}}_{\mathrm{q}_{\mathrm{m_xj}}}\left[\underline{\mathbf{x}}_{\mathrm{q}}(\mathrm{k})\right] + \xi_{\mathrm{m_xj}}(\mathrm{k}) \right\} - \rho_{\mathrm{m_x}} \end{bmatrix} \tag{34}$$

$$\underline{\mathbf{Q}}_{\mathbf{H}}(\mathrm{k}) \triangleq \begin{bmatrix} -\sum_{\mathrm{j}=1}^{\mathrm{m}_\sigma} \eta_{1\mathrm{j}} \left\{ \mathrm{x}_{\mathrm{r}_{1\mathrm{j}}}(\mathrm{k}) - \widehat{\mathrm{x}}_{r_{1\mathrm{j}}}(\mathrm{k}) + \widehat{\mathrm{g}}_{1\mathrm{j}}(\mathrm{k}) + \widehat{\mathrm{f}}_{\mathrm{q}_{1\mathrm{j}}}\left[\underline{\mathbf{x}}_{\mathrm{q}}(\mathrm{k})\right] + \xi_{1\mathrm{j}}(\mathrm{k}) \right\} + \rho_i \\ \vdots \\ -\sum_{\mathrm{j}=1}^{\mathrm{m}_\sigma} \eta_{\mathrm{m_xj}} \left\{ \mathrm{x}_{\mathrm{m_xj}}(\mathrm{k}) - \widehat{\mathrm{x}}_{\mathrm{m_xj}}(\mathrm{k}) + \widehat{\mathrm{g}}_{\mathrm{m_xj}}(\mathrm{k}) + \widehat{\mathrm{f}}_{\mathrm{q}_{\mathrm{m_xj}}}\left[\underline{\mathbf{x}}_{\mathrm{q}}(\mathrm{k})\right] + \xi_{\mathrm{m_xj}}(\mathrm{k}) \right\} + \rho_{\mathrm{m_x}} \end{bmatrix} + \left\{ \sum_{\mathrm{j}=1}^{\mathrm{m}_\sigma} \begin{bmatrix} \eta_{1\mathrm{j}} & \cdots & 0 \\ \vdots & \ddots & \vdots \\ 0 & \cdots & \eta_{\mathrm{m_x,j}} \end{bmatrix} \left[\boldsymbol{\Gamma}_{\mathrm{j}}(\mathrm{k}-1) \widehat{\mathbf{B}}_{\mathrm{j}}\,(\mathrm{k}-1) \right] \right\} \underline{\mathbf{u}}\,(\mathrm{k}-1) \tag{35}$$

Hence, control input is calculated according to Eq. (36).

$$\begin{aligned} \underline{\mathbf{u}}(\mathrm{k}) &= [1-\alpha(\mathrm{k})]\,\mathbf{B}^{-1}(\mathrm{k})\underline{\mathcal{Q}}_{\mathrm{L}}(\mathrm{k}) + \alpha(\mathrm{k})\mathbf{B}^{-1}(\mathrm{k})\underline{\mathcal{Q}}_{\mathrm{H}}(\mathrm{k}) \\ \underline{\mathcal{Q}}_{\mathrm{L}}(\mathrm{k}) &= \left\{ \sum_{\mathrm{j}=1}^{\mathrm{m}_\sigma} \begin{bmatrix} \eta_{1\mathrm{j}} & \cdots & 0 \\ \vdots & \ddots & \vdots \\ 0 & \cdots & \eta_{\mathrm{m_x,j}} \end{bmatrix} \left[\mathbf{I} + \Gamma_{\mathrm{j}}(\mathrm{k}) \right] \hat{\mathbf{B}}_{\mathrm{j}}(\mathrm{k}) \right\}^{-1} \underline{\boldsymbol{q}}_{\mathrm{L}}(\mathrm{k}) \\ \underline{\mathcal{Q}}_{\mathrm{H}}(\mathrm{k}) &= \left\{ \sum_{\mathrm{j}=1}^{\mathrm{m}_\sigma} \begin{bmatrix} \eta_{1\mathrm{j}} & \cdots & 0 \\ \vdots & \ddots & \vdots \\ 0 & \cdots & \eta_{\mathrm{m_x,j}} \end{bmatrix} \left[\mathbf{I} + \Gamma_{\mathrm{j}}(\mathrm{k}) \right] \hat{\mathbf{B}}_{\mathrm{j}}(\mathrm{k}) \right\}^{-1} \underline{\boldsymbol{q}}_{\mathrm{H}}(\mathrm{k}) \end{aligned} \tag{36}$$

Proposition 3 ends here.

Remark 6 (Control system design parameters recommendation). Regarding controller performance tuning, appropriate selection of design parameters η_{ij},μ_{i},λ_{ij} and $\alpha(\mathrm{k})$ are essential for obtaining the best performance. η_{ij} represents weight factor for each switching configuration. It is strongly recommended to opt for higher values in case of severe switching cases. μ_{i} defines how fast system dynamics converge to the sliding surface of $\boldsymbol{\Omega}_{\mathrm{i}}$. Thus selecting greater values provide a smooth transition toward the sliding surface. $\alpha(\mathrm{k})$ determines system dynamics proximity with respect to stability bounds. Proximity factor selection highly depends upon uncertainty approximation accuracy. In fact, if total uncertainties are ideally approximated, the middle point that is, $\alpha(\mathrm{k}) = 0.5$ usually results in best performance otherwise the appropriate value is to be found through trial and error. λ_{ij} incorporates tracking performance and overall stability of closed-loop system such that selecting values around stability borders ($\left|\lambda_{\mathrm{ij}}\right| = 1$) results in superior stability but poor tracking performance and vice versa.

It is observed that control input bounds are calculated based on the rigid model of system, desired reference values, and approximated uncertainties from FEA. In the reaching phase, Lyapunov stability condition is based on the selection of inputs in appropriate bounds according to Eq. (23). After reaching sliding mode, control input bounds are selected such that closed-loop system will reside within the sliding band according to Eq. (36). In other words, by following the detailed procedure, it is ensured

https://doi.org/10.1017/S0263574721001004 Published online by Cambridge University Press

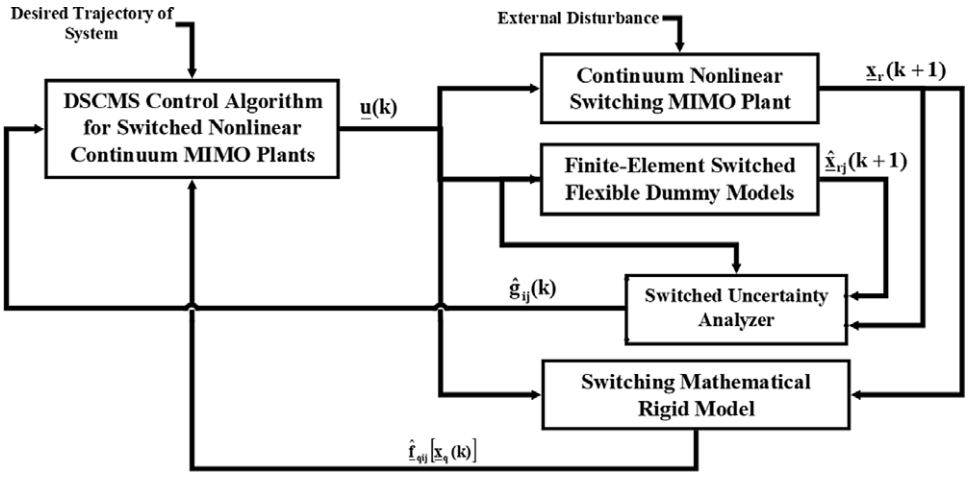

Fig. 1. *Flowchart of DSCMS control algorithm.*

that the system will reach sliding surface in finite time and remains there afterward. Therefore, the control signal is not calculated through a switching signal like the conventional continuous-time SMC approach and the effects of input chattering will no longer exist.

Summarizing the previous steps, the algorithm for Discrete-Time Sliding mode Control of Uncertain Continuum Mechanics Switched MIMO systems (DSCMS) is listed as follows:

(a) Deriving mathematical rigid model of the real system using nominal parameters for each switching configuration.

(b) Discretizing the rigid model to obtain $\hat{g}_{ij}(k)$ and $\hat{\mathbf{B}}_j(k)$.

(c) Setting up the dummy models for each switching configuration to approximate parametric and unstructured uncertainties.

(d) Adjusting initial control weighting parameters η_{ij}, finite-time convergence factor μ_i, proximity factor $\alpha(k)$ and sliding function parameters λ_{ij} through investigation over acceptable reference error ranges, system response behavior over different DOFs, and tracking priorities according to Remark 6.

(e) Calculating stability bounds according to Theorem 1, Propositions 1 and 3.

(f) Applying DSCMS control input through appropriate selection of control proximity factor $\alpha(k)$.

In Fig. 1, the general block-diagram of the proposed DSCMS algorithm illustrating the operation logic of the feedback system in cases where flexibility of switching system is excited by control commands, is depicted.

4. Numerical Example

This section demonstrates controller performance and effectiveness through FEA Simulation for a continuum mechanics switched MIMO system. The selected flexible mechanism which is located on a horizontal plane consists of two flexible beams fixed to each other in the center and carries four concentrated masses attached to either end of each beam according to Fig. 2. A nonlinear van der pol oscillator is also attached to the mechanism Center of Gravity (COG) to increase system nonlinearity for control system evaluation. The proposed mechanism could be represented as a simplified model of a quadrature, space station, or other similar applications. Nevertheless, its capability of demonstrating the deteriorating effect of continuum mechanics vibration in the control process was the main motivation to use it for the evaluation of DSCMS.

https://doi.org/10.1017/S0263574721001004 Published online by Cambridge University Press

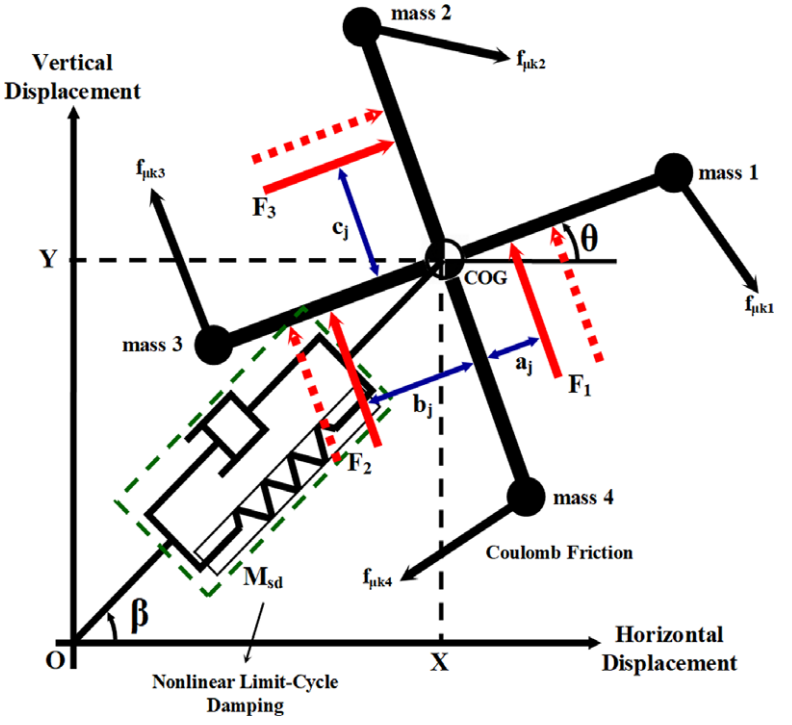

Fig. 2. *Schematic description of the investigated dynamical system. Systems parameters and geometry are similar to the model of study [20].*

The control objective is to guide the system such that its COG follows a predefined trajectory. Since the entire motion takes place in a horizontal plane, the mechanism would have three DOFs and three subsequent subsystems would be available throughout the development of DSCMS. To obtain the squared system described in Assumption 1, three concentrated forces as control inputs are applied in arbitrary positions over beam lengths and friction forces are exerted in the location of point masses. Proposed control system verification regarding switching dynamics could be investigated from various aspects. However, without loss of generality, switching is assumed to take place between force exertion points. Two different configurations are simulated such that in the first configuration, control input forces are exerted at the very end of beams close to concentrated masses and in the second configuration, exertion points will be chosen near COG.

The closed-loop system is modeled in the FEA framework in a multitude of details to accurately simulate physical implementation. These details include mechanical strength properties such as elasticity and Poisson ratio, geometric sections, Coulomb friction, and other simulation preliminaries. The whole process necessitates the transformation of control algorithm codes into ANSYS® mechanical APDL macros for use in transient analysis. Auxiliary dummy models are also constructed in FEA and run alongside the system sharing identical control reference values, initial position for each solution time step, and controller design parameters with the exception that their geometry and mechanical properties are defined according to known nominal values. Table I defines parameters used for both real system (within parentheses) and dummy models in simulation setup:

Dynamical equations regarding the mathematical rigid model of proposed mechanism are comprehensively expressed in the author's previous study [20] and only simulation results of the closed-loop system are analyzed here. Two dummy models corresponding to each switching configuration of force exertion point are constructed to estimate model uncertainties according to Remark 3. It should be noted that dummy models are stimulated with the same control input forces applied on the real system and their initial position is set exactly similar to the system initial position for every solution time step. Figure 3

https://doi.org/10.1017/S0263574721001004 Published online by Cambridge University Press

Table I. *Parameters for simulation setup.*

Parameter	Definition	Value
m, m_0	Concentrated masses and their nominal value	2.2 (2.0) [kg]
K, K_0	Elastic coefficient of van der pole oscillator and its nominal value	5.0 (10) [N/m]
C_v, C_{v_0}	Damping coefficient of van der pole oscillator and its nominal value	10 (15) [N.s/m]
μ, μ_0	Coulomb friction coefficient and its nominal value	0.15 (0.2)
l, l_0	Distance from COG to any of concentrated masses and its nominal value	1.1 (1) [m]
ρ, ρ_0	Beams mass density for aluminum and its nominal value	2600 (2700) [kg/m^3]
A	Beams cross-section (Height × Width)	90 × 20 mm
E	Elastic modulus for aluminum	69 × 10^9 [N/m^2]
ν	Poisson ratio for aluminum	0.32
X_0, Y_0, θ_0	System initial position	1 [m] , 1 [m] , 0 [Rad]
a_1, b_1, c_1	Control inputs exertion position for first switch	
a_2, b_2, c_2	Control inputs exertion position for second switch	
α	Control proximity factor	0.5
T	Sampling time	0.01sec

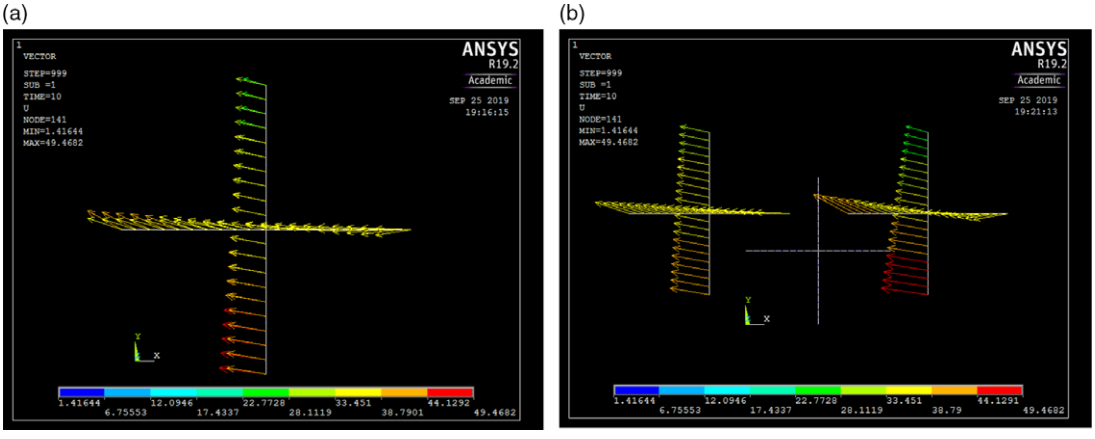

Fig. 3. *Nodal displacement vector analysis for dummy models corresponding to each switching configuration. (a) Dummy models coincided in the center. (b) Dummy models regarding each switching configuration.*

shows different system behavior for either dummy model responding to identical initial condition and input force though with different force exertion points. In Fig. 3(a), both models are coincided in the center to clearly demonstrate the differences in magnitude and orientation of each node displacement vector.

For better graphical representation of dummy models regarding to each switching configuration, Fig. 3(b) shows the separated velocity vector fields of the dummy models computed by ANSYS.

Switching signal is depicted in Fig. 4 in which dwell time is set to 2.5 s for the current simulation.

Figure 5 depicts closed-loop system response comparison in tracking sinusoidal references $X_d = 2.0 \sin 0.6\pi t$, $Y_d = 2 \sin 0.4\pi t$ and $\theta_d = 0.1\pi \sin 0.2\pi t$ and alongside with their respective derivatives for horizontal (Fig. 5(a), (b)), vertical (Fig. 5(c), (d)), and angular (Fig. 5(e), (f)) degrees of freedom. Simulation results are compared with those of FEA-based controllers (Discrete Sliding Mode Controller

https://doi.org/10.1017/S0263574721001004 Published online by Cambridge University Press

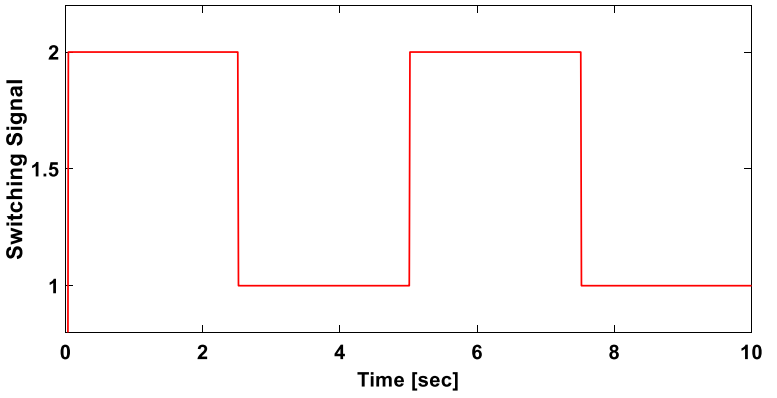

Fig. 4. *Switching signal that alters force exertion points throughout the flexible arms.*

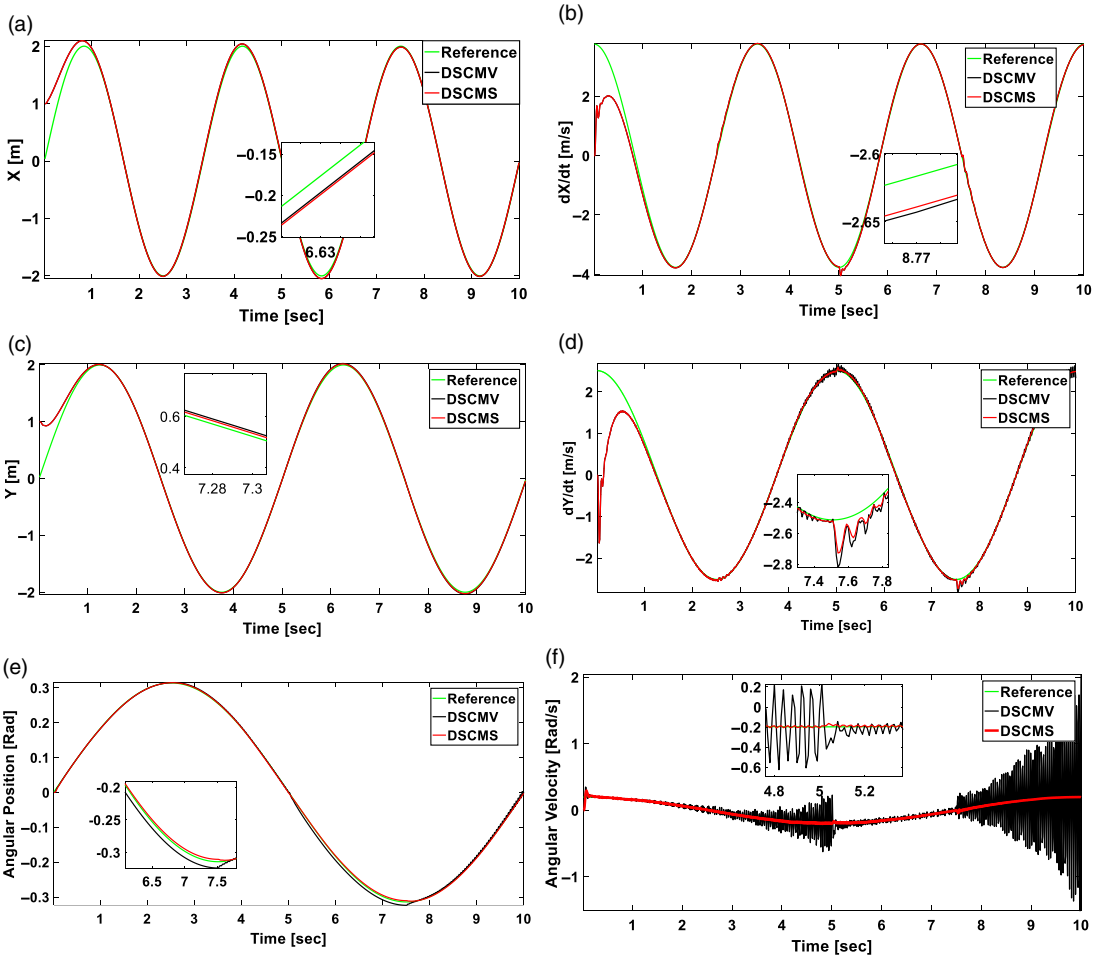

Fig. 5. *Time history plots of the response comparison of flexible system (a) Horizontal position of COG. (b) Horizontal velocity of COG. (c) Vertical position of COG. (d) Vertical velocity of COG. (e) Angular displacement. (f) Angular velocity.*

https://doi.org/10.1017/S0263574721001004 Published online by Cambridge University Press

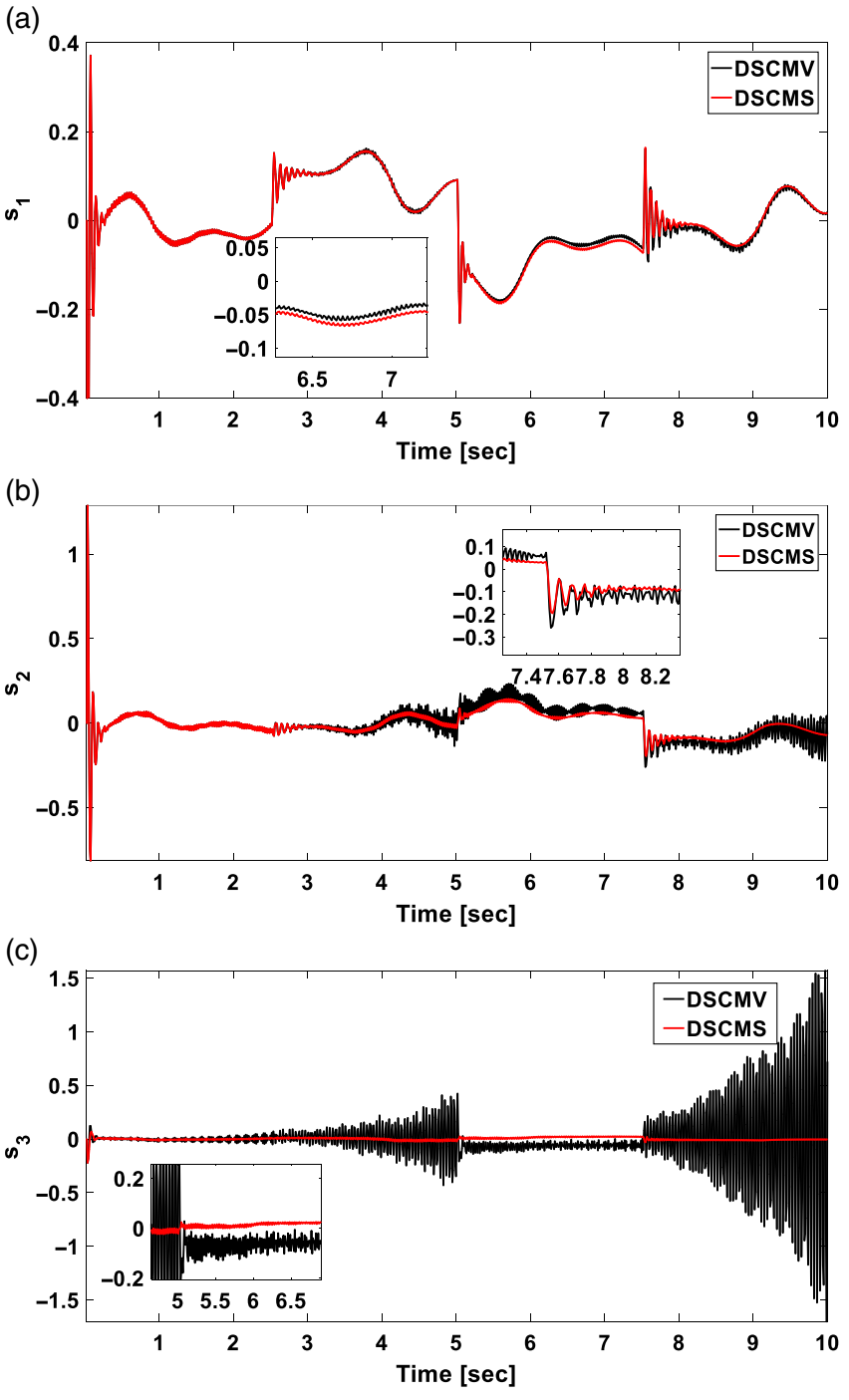

Fig. 6. *Deviation of sliding functions comparison (a) s_{11}. (b) s_{12}. (c)s_{21}*

for MIMO Vibrational Systems abbreviated as DSCMV) presented in [20], which does not include switching effects in the construction of control algorithm.

It is observed that the reference values are successfully tracked for DSCMS closed-loop system despite frequent switches altering control input force exertion points. It is also notable that system response undergoes a brief disturbance right after switching moment but the controller immediately

https://doi.org/10.1017/S0263574721001004 Published online by Cambridge University Press

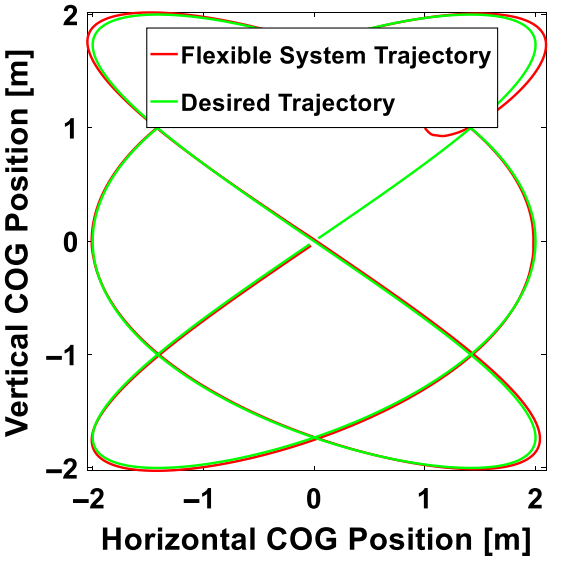

Fig. 7. *Path tracking of COG for MIMO flexible system.*

drives the system into reference trajectories. Since switching alters the exertion point of input forces and does not influence their magnitude, system horizontal and vertical motion is less affected after switching. In this comparison, the DSCMV controller algorithm is constructed based on the worst switching case (when input forces are closer to origin) to satisfy stability conditions for less critical cases. Nevertheless, the closed-loop system becomes unstable due to the fact that adapting controller inputs stability bounds to more critical switching cases, typically results in severe deformations which rule out system linearity. These nonlinear behaviors are oftentimes too quick to be detectable by the FEA estimator. In theory, the issue could be addressed by the increasing sampling rate. However, smaller sampling period results in further complications such that increasing data reading rate involves high-frequency modes and inaccurate control signal calculation.

Figure 6 illustrates sliding surface fluctuations around origin in period of simulation for horizontal (Fig. 6(a)), vertical (Fig. 6(b)), and angular (Fig. 6(c)) motions. Clearly, there is no sign of high-frequency zigzag motion around the sliding surface. In fact, the selection of control inputs between stability bounds totally removes the chattering effect (which is normally seen in SMC techniques) without notable performance compromise. Presence of model uncertainties justifies the deviation of sliding functions from the origin which is notably reduced in DSMCS closed-loop response.

Path tracking of system COG is depicted in Fig. 7. In this figure, it is observed that planar motion of the mechanism follows the desired path, which was expected based on precise trajectory tracking of state values illustrated in Fig. 5.

Figure 8 represents controller inputs that is required to stabilize the close-loop system under switching signal is depicted in Fig. 4. The superiority of DSCMS controller performance stands out regarding both chattering effects and control effort. Minor fluctuations are observed after each switching period which is quickly compensated through the controller effort to reach the sliding surface.

5. Conclusion

In this paper, a new approach in the control of continuum mechanics MIMO uncertain switched system considering unknown time delay and active switching configuration is presented. The control algorithm is constructed based on discrete sliding mode theorem and model uncertainties are estimated via Finite Element Analysis. Candidate Lyapunov function is proposed according to a set of sliding functions

https://doi.org/10.1017/S0263574721001004 Published online by Cambridge University Press

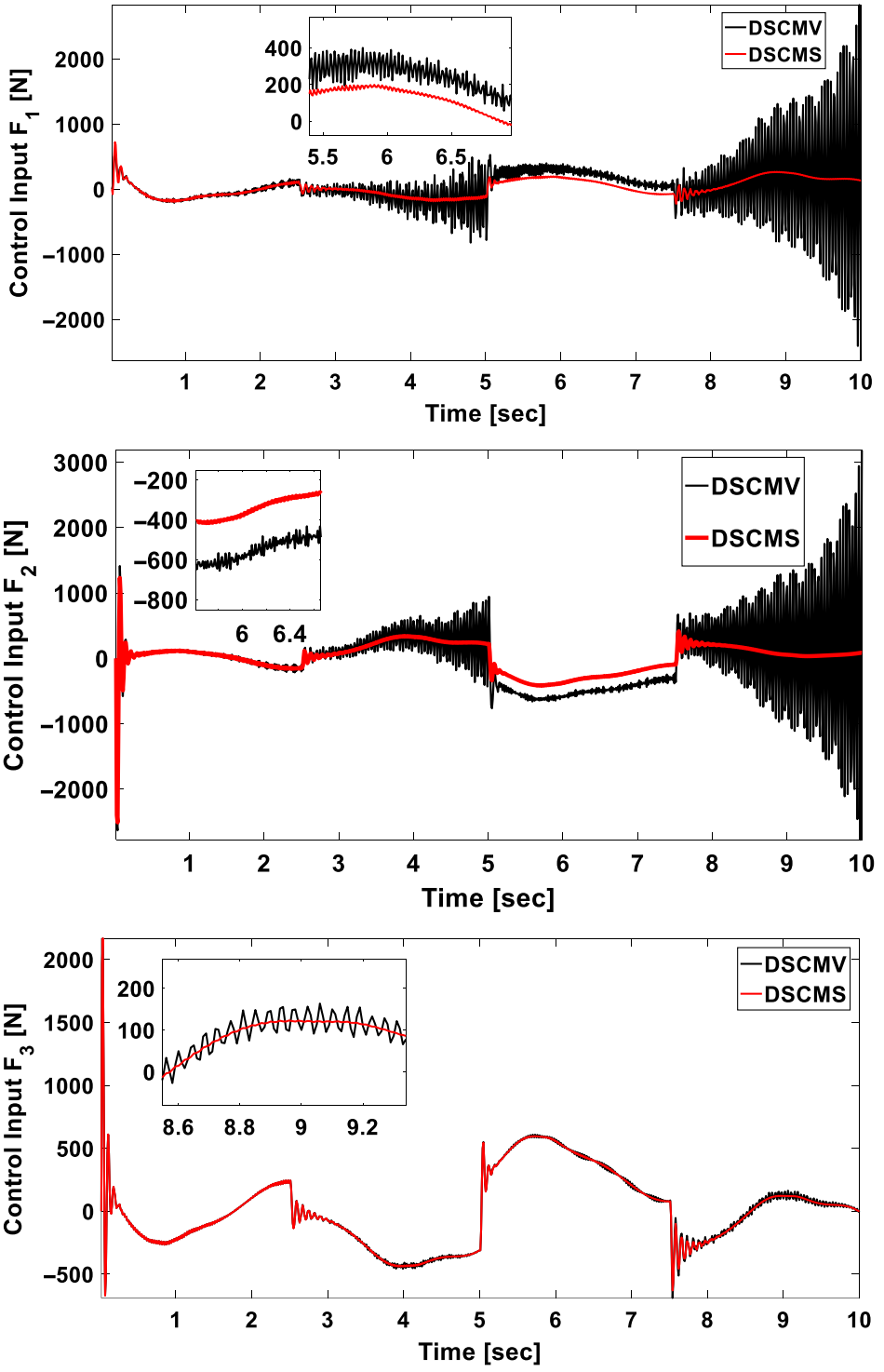

Fig. 8. *Control input forces required to track desired references.*

https://doi.org/10.1017/S0263574721001004 Published online by Cambridge University Press

corresponding to each individual subsystem and given switching configuration while Krasovskii terms are included in case the system is affected by time delay. Controller inputs are then calculated to reside within stability bounds derived from the Lyapunov stability criterion. Proposed control algorithm performance in comparison with available methods in the existing literature is verified through FEA simulations.

Future works recommendation

In this paper, tracking control of continuum mechanics systems has been investigated regardless of vibration level. However, FEA-based approximation method presented in this paper is not always accurate due to numerical methods complications. These inaccuracies directly affect the calculation of control input bounds increasing the possibility of driving system dynamics outside the stability region. To address this issue, the following approaches are recommended for future references:

- Using vibration suppression methods simultaneously alongside proposed DSCMS to attenuate system vibrations in order to avoid intensification of unstructured uncertainties.
- Compressing stability margins to ensure asymptotic stability in case of inaccurate uncertainty approximation.

Competing Interest. The authors of this manuscript are the members of the Department of Mechanical Engineering, K. N. Toosi University of Technology, and are not employed by any non-academic government agencies. Also, they are not dependent upon funding or data from any political, military, or sovereignty corporation or organization.

References

[1] J.-J. E. Slotine, W. Li, *Applied Nonlinear Control* (Prentice Hall, Englewood Cliffs, New Jersey, 1991).
[2] S. S. Rao, *Vibration of Continuous Systems* (John Wiley & Sons, Inc., Hoboken, New Jersey, 2007).
[3] D. Liberzon, *Switching in Systems and Control* (Birkhäuser, Boston, 2003).
[4] S. Huang and Z. Xiang, "Finite-time output tracking for a class of switched nonlinear systems," *Int. J. Robust Nonlinear Control*. **56**, 1920–1924 (2016). doi: 10.1002/rnc.3616.
[5] D. Yang, Y. Liu and J. Zhao, "Guaranteed cost control for switched LPV systems via parameter and state-dependent switching with dwell time and its application," *Optim Control Appl Methods.* **38**, 601–617 (2017). doi: 10.1002/oca.2274.
[6] J. L. Wu, "Stabilizing controllers design for switched nonlinear systems in strict-feedback form," *Automatica.* **45**, 1092–1096 (2009). doi: 10.1016/j.automatica.2008.12.004.
[7] D. Zhai, L. An and Q.L. Zhang, "Adaptive asymptotic stabilization of switched parametric strict-feedback systems with switched control," *Int J Robust Nonlinear Control.* **28**, 3422–3434 (2018). doi: 10.1002/rnc.4089.
[8] M. L. Chiang and L. C. Fu, "Adaptive stabilization of a class of uncertain switched nonlinear systems with backstepping control," *Automatica.* **50**, 2128–2135 (2014). doi: 10.1016/j.automatica.2014.05.029.
[9] L. Zhang, L. Nie, B. Cai, S. Yuan and D. Wang, "Switched linear parameter-varying modeling and tracking control for flexible hypersonic vehicle," *Aerosp Sci Technol.* **95**, 105445(2019). doi: 10.1016/j.ast.2019.105445.
[10] M. R. Homaeinezhad and S. Yaqubi, "Discrete-time sliding-surface based control of parametrically uncertain nonlinear systems with unknown time-delay and inaccessible switching mode detection," *Int J Control.* 1–37 (2019). doi: 10.1080/00207179.2019.1605205.
[11] L. Zhou and G. Chen, "Fuzzy sliding mode control of flexible spinning beam using a wireless piezoelectric stack actuator," *Appl Acoust.* **128**, 40–44 (2017). doi: 10.1016/j.apacoust.2017.06.015.
[12] W. Hu, Y. Gao and B. Yang, "Semi-active vibration control of two flexible plates using an innovative joint mechanism," *Mech Syst Signal Process*. **130**, 565–584 (2019). doi: 10.1016/j.ymssp.2019.05.034.
[13] A. Kater and T. Meurer, "Motion planning and tracking control for coupled flexible beam structures," *Control Eng. Pract.* **84**, 389–398 (2019). doi: 10.1016/j.conengprac.2018.12.012.
[14] Q. Zhang, C. Li, J. Zhang and J. Zhang, "Smooth adaptive sliding mode vibration control of a flexible parallel manipulator with multiple smart linkages in modal space," *J Sound Vib.* **411**, 1–19 (2017). doi: 10.1016/j.jsv.2017.08.052.
[15] M. R. Homaeinezhad, F. FotoohiNia and H. M. Gholyan, "Controlling uncertain nonlinear structural vibrations of moving continuum systemby embedding a vibration monitoring unit to feedback algorithm," *Struct Control Health Monit*. (2020). doi: 10.1002/stc.2626.
[16] M. R. Homaeinezhad, F. FotoohiNia and S. Yaqubi, "Active predictive vibration suppression algorithm for structural stability and tracking control of nonlinear multivariable continuum-mechanics mobile systems," *Optim Control Appl Methods.* 1–23 (2020). doi: 10.1002/oca.2687.
[17] E. Franco, A. Astolfi and F. Rodriguez y Baena, "Robust balancing control of flexible inverted-pendulum systems," *Mech Mach Theory.* **130**, 539–551 (2018). doi: 10.1016/j.mechmachtheory.2018.09.001.

[18] B. Chen, J. Huang and J. C. Ji, "Control of flexible single-link manipulators having Duffing oscillator dynamics," *Mech Syst Signal Process.* **121**, 44–57 (2019). doi: 10.1016/j.ymssp.2018.11.014.
[19] K. Bendine, F. B. Boukhoulda, M. Nouari and Z. Satla, "Active vibration control of functionally graded beams with piezoelectric layers based on higher order shear deformation theory," *Earthq Eng Eng Vib.* **15**, 611–620 (2016). doi: 10.1007/s11803-016-0352-y.
[20] M. R. Homaeinezhad, S. Yaqubi and F. FotoohiNia, "FEA based discrete-time sliding mode control of uncertain continuum mechanics MIMO vibrational systems," *J Sound Vib.* **460**, 114902 (2019). doi: 10.1016/j.jsv.2019.114902.
[21] S. Ghasemi-Moghadam and M. R. Homaeinezhad, "Attitude determination by combining arrays of MEMS accelerometers, gyros, and magnetometers via quaternion-based complementary filter," *Int J Numer Model Electron Networks Devices Fields.* **31**, 1–24 (2018). doi: 10.1002/jnm.2282.
[22] S. Yaqubi and M. R. Homaeinezhad, "Optimally designed Lyapunov–Krasovskii terminal costs for robust stable–feasible model predictive control of uncertain time-delay nonlinear dynamical systems," Proc IMechE Part I. (2020). doi:/10.1177/0959651820952193.

Cite this article: M. R. Homaeinezhad and F. FotoohiNia (2022). "FEA-based tracking control of flexible body switching dynamic structure", Robotica **40**, 1168–1187. https://doi.org/10.1017/S0263574721001004